Proceedings of the 7th International Symposium on Cavitation
CAV2009 – Paper No. 138
August 17-22, 2009, Ann Arbor, Michigan, USA

A dual-time implicit preconditioned Navier-Stokes method for solving 2D steady/unsteady laminar cavitating/noncavitating flows using a Barotropic model

Kazem Hejranfar
Department of Aerospace Engineering
Sharif University of Technology, Tehran, Iran
khejran@sharif.edu

Eslam Ezzatneshan
Department of Aerospace Engineering
Sharif University of Technology, Tehran, Iran
ezzatneshan@ae.sharif.edu

Kasra Fattah Hesary
Department of Aerospace Engineering
Sharif University of Technology, Tehran, Iran
kasra.fattah@gmail.com

ABSTRACT

A two-dimensional, time-accurate, homogeneous multiphase, preconditioned Navier-Stokes method is applied to solve steady and unsteady cavitating laminar flows over 2D hydrofoils. A cell-centered finite-volume scheme employing the suitable dissipation terms to account for density jumps across the cavity interface is shown to yield an effective method for solving the multiphase Navier-Stokes equations. This numerical resolution is coupled to a single-fluid model of cavitation that the evolution of the density is governed by a barotropic sate law. A preconditioning strategy is used to prevent the system of equations to be stiff. A dual-time implicit procedure is applied for time accurate computation of unsteady cavitating flows. A sensitivity study is conducted to evaluate the effects of various parameters such as numerical dissipation coefficients and preconditioning on the accuracy and performance of the solution. The computations are presented for steady and unsteady laminar cavitating flows around the NACA0012 hydrofoil for different conditions. The solution procedure presented is shown to be accurate and efficient for predicting steady/unsteady laminar cavitating/noncavitating flows over 2D hydrofoils.

INTRODUCTION

Cavitation can occur in a wide range of flows and this physical process is of particular interest for studying marine propellers, water crafts, turbine blades and low speed centrifugal pumps. This phenomenon strongly affects the flow field, the neighbouring structures and it plays an important role in the design of hydrodynamic machines. Several physical and numerical models have been developed to investigate steady cavitating flows. The reason for the absence of a more detailed explanation of the physics of cavitation is, of course, the need for a discussion of the unsteady viscous cavitating flow phenomena. The shape and collapse of the vapor structures usually fluctuate in time and this unstable behavior causes to be important for understanding of unsteady two-phase flow structure of cavitation. Most studies for unsteady cavitating flows known in the literatures are performed for turbulent flows, and a little work can be found for laminar flows. The lift disintegration is a major flow feature in cavitating flows and is due to the increased bubble size on the hydrofoil. Since the lift and especially drag calculations depend on viscous effects, thus the choice of turbulence model has a strong impact on the results. There is no widely acceptable turbulence model that can handle the uncertainties of unsteady cavitating two-phase flows. Inspection of the studies on laminar cavitating flows making it possible to model cavitation behavior in a physically more realistic manner.

A numerical analysis of cavitating flow of viscous fluid is a challenging computational problem. In fact, one has to deal with localized large variations of density which are present within a predominantly incompressible liquid medium, interactions between phases, turbulence, irregularly shaped interfaces, compressibility effects and the stiffness in the numerical model. A number of different approaches have been developed to investigate cavitation numerically. Kueny et al. [1] described the vapor/liquid interface as a stream sheet at constant static pressure equal to the vapor pressure and simulated the steady sheet cavitation. Kubota et al. [2] described the behavior of small gas bubbles in the fluid by the Rayleigh-Plesset equation with the changing pressure field. Delannoy and Kueny [3] assumed that the liquid and gas phases are represented by a single continuous equation of state that strongly links the mixture density to the static pressure. This barotropic flow model has been applied by Song et al. [5] and

produced the results that agree very well with the experimental data and observations. (see Arndt et al. [6]). Several modifications have been investigated by Reboud et al. [7] and Coutier-Delgosha et al. [8,9,13] to improve this physical model. Merkle et al. [4] and Kunz et al. [10] proposed another development with considering two mass balance equations for liquid and vapor, instead of a single equation for mixture. Some papers deal with this topic that numerically simulated the laminar cavitating flows on pumps or low speed propeller blades. For example, Frobenius et al. [11] presented a numerical simulation of cavitating flow through a low speed impeller. Ventikos et al. [12] developed a numerical method that is based on a viscous flow solver and they examined it for the simulation of steady and unsteady laminar cavitating flows.

The main objective of the present study is to develop an efficient and accurate flow solver for computing steady/unsteady cavitating laminar flows. Herein, a dual-time implicit preconditioned Navier-Stokes method is used for this propose. A central difference finite volume method in conjunction with the modified Jameson's type dissipation terms to account for density jumps across the cavity interface is employed to solve the multiphase Navier-Stokes equations. The development of cavitation is imposed and controlled through the evolution of the vapor pressure used in the cavitation model. A barotropic state law is applied to model steady/unsteady cavitating flow. This model considers the liquid-vapor mixture as a single fluid, characterized by a density that varies according to a state law. It is assumed that locally the velocities are the same for liquid and vapor in the interface and the interface is considered to be in a dynamic equilibrium. To validate the numerical results, the steady/unsteady noncavitating laminar flows are computed by setting a high cavitation number and the results for the NACA 0012 hydrofoil are compared with the numerical solution by Hafez et al. [14]. Then, the steady/unsteady cavitating flow patterns over the NACA0012 hydrofoil at different conditions are presented. The influence of the numerical parameters such as dissipation terms on the results is also investigated and the overall capability and performance of the present modeling are assessed. The effects of preconditioning on the convergence rate of the solution of the cavitating flows are also examined. Some observations are presented concerning the unsteady cavitation flow condition. The results predicated by steady and unsteady cases are compared with the available results. The study shows that the numerical treatment is efficient and accurate for computing the steady/unsteady laminar noncavitating/cavitating flows over 2D hydrofoils.

PROBLEM FORMULATION

By assumption of thermal and dynamic equilibrium for the homogeneous single fluid approach, the Navier-Stokes equations are used to model cavitating flows without considering the energy conservation equation. The barotropic state law relates the pressure and density variables and completes the set of equations. The Navier-Stokes equations are written in the vector form as follows:

$$\frac{\partial U}{\partial \tau}+\frac{\partial F}{\partial x}+\frac{\partial G}{\partial y}=\frac{\partial F_v}{\partial x}+\frac{\partial G_v}{\partial y} \tag{1}$$

Here τ is the pseudo time-step. U is the vector of dependent variables, F and G are the invicid fluxes and F_v and G_v are the viscous fluxes. This formulation is devoted to highly compressible flows. In cavitation flows that the most region of the flow field are low-compressible or incompressible, the efficiency of the formulation decreases dramatically, because the order of convective and acoustic eigenvalues becomes very different that makes the system of equations to be stiff. To rectify this problem, a preconditioning strategy is used. It consists in multiplying the temporal derivatives in the continuity equation by a preconditioning to obtain a well-conditioned system. A pseudo time-derivative term of density is introduced in the equations from the work of Chorin [15]:

$$\frac{\partial \rho_m}{\partial \tau}=\frac{\partial \rho_m}{\partial p}\frac{\partial p}{\partial \tau} \tag{2}$$

$$\frac{\partial \rho_m}{\partial p}=\beta^2 \tag{3}$$

where β is the isothermal speed of sound and it is known as the pseudo-compressibility coefficient or the preconditioning parameter. To obtain an efficient time-marching numerical scheme, β is selected in such a manner that to rescale the eigenvalues of the system such that the acoustic speeds are of the same order of the local convective velocities [16]. The resulting preconditioned multiphase Navier-Stokes equations can be expressed as:

$$\Pi\frac{\partial Q}{\partial \tau}+\frac{\partial F}{\partial x}+\frac{\partial G}{\partial y}=\frac{\partial F_v}{\partial x}+\frac{\partial G_v}{\partial y} \tag{4}$$

$$Q=\begin{bmatrix}p\\u\\v\end{bmatrix},F=\begin{bmatrix}\rho_m u\\ \rho_m u^2+p\\ \rho_m uv\end{bmatrix},G=\begin{bmatrix}\rho_m v\\ \rho_m uv\\ \rho_m v^2+p\end{bmatrix},$$
$$F_v=\begin{bmatrix}0\\ \tau_{xx}\\ \tau_{xy}\end{bmatrix},G_v=\begin{bmatrix}0\\ \tau_{yx}\\ \tau_{yy}\end{bmatrix} \tag{5}$$

where p is the pressure, u and v are the flow velocities and τ_{ij} is the viscous stress tensor. Turkel [17] modified this preconditioning strategy by adding corresponding artificial time-derivative term to the momentum equations and introduced a coefficient such as α_u. Coutier-Delgosha [13] computed the α_u locally according to the local void fraction α as follows:

$$\alpha_u=\begin{cases}1 & if\ \alpha=0\ \ or\ \ \alpha=1\\ |2\alpha-1| & if\quad 0<\alpha<1\end{cases} \tag{6}$$

$$\alpha=\frac{\rho_l-\rho_m}{\rho_l-\rho_v} \tag{7}$$

The subscripts *l* and *v* stand for the properties of pure liquid and pure vapor, which are assumed to be constant and ρ_m is the mixture density. Herein, the influence of these coefficients on the numerical results is investigated. Note that these terms are of no physical meaning and they are cancelled at steady

state; thus they have no effect on the solution. The preconditioning matrix Π is given by:

$$\Pi = \begin{bmatrix} \frac{1}{\beta^2} & 0 & 0 \\ \alpha_u \frac{u}{\beta^2} & \rho_m & 0 \\ \alpha_u \frac{v}{\beta^2} & 0 & \rho_m \end{bmatrix} \tag{8}$$

For simulation of the unsteady periodic nature of flows, a second-order implicit dual-time procedure is used [18]. In this method, the terms regarding the real time derivatives are considered in the system of equations and Eq. (6) is rewritten as follows:

$$\frac{\partial U}{\partial t} + \Pi \frac{\partial Q}{\partial \tau} + \frac{\partial F}{\partial x} + \frac{\partial G}{\partial y} = \frac{\partial F_v}{\partial x} + \frac{\partial G_v}{\partial y} \tag{9}$$

where, t is the physical time step and U is defined as:

$$U = \begin{pmatrix} \rho \\ \rho u \\ \rho v \end{pmatrix} \tag{10}$$

The integral form of the preconditioning multiphase Navier-Stokes equations using the Gauss divergence theorem for an arbitrary control volume Ω is written as:

$$\frac{\partial}{\partial t}\iint_{\Omega} U d\Omega + \frac{\partial}{\partial \tau}\iint_{\Omega} \prod Q d\Omega + \oint \vec{H} \cdot \hat{n} d\ell - \oint \vec{H}_v \cdot \hat{n} d\ell = 0 \tag{11}$$

Here, H and H_v are the total inviscid and viscous flux vectors, respectively.

CAVITATION MODEL

In the present work, the two-phase flow is considered as only one fluid in which the variation of density in the flow field is governed by a barotropic state law [3,7-9,13]. The barotropic model is based on the assumption of the thermodynamic equilibrium and the neglect of velocity slip between liquid and vapor phases. Two phase fluid is considered as a single fluid in which the density varies from the liquid to the vapor with respect to the local static pressure. The barotropic state law $\rho(p)$ is shown in Fig. 1. When the pressure is higher or lower than the vapor pressure (p_{vap}), the fluid is considered as purely liquid or vapor, and a continuous variation of density between liquid and vapor phases is evaluated by using a sinusoidal curve as follows:

$$\rho_m = \frac{\rho_l + \rho_v}{2} + \frac{\rho_l - \rho_v}{2} \times Sin\left(\frac{2}{\rho_l - \rho_v} \frac{p - p_{vap}}{c^2_{min}}\right) \tag{12}$$

where $1/c^2_{min}$ is the maximum slop of the curve that occurs at the vapor pressure and $c_{min} = \sqrt{\partial p / \partial \rho}$ is the minimum speed of sound in the mixture. The measurement of speed of sound in cavitating flows is difficult and its value usually is set to be constant in computational approaches. It should be noted that the different value of c_{min} can significantly affect the results of numerical simulation [19,20].

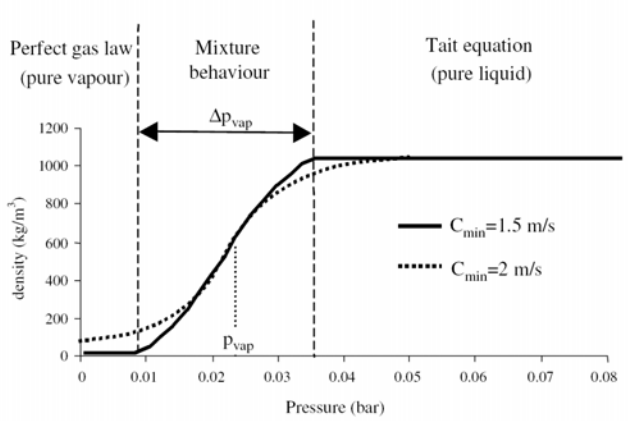

Figure 1: The barotropic state law $\rho(p)$ [13].

NUMERICAL TREATMENT

The governing equations are descretized using a central difference finite volume scheme and the domain is divided into a finite number of structured quadrilateral cells. The discrete form of Eq. (11) over a computational cell volume becomes:

$$\frac{d}{d\tau}(Q_j A_j) + R(Q_j) = 0 \tag{13}$$

where A_j is the cell area and $R(Q_j)$ is the residual vector defined as:

$$R(Q_j) = \Pi_j^{-1}\left(\sum_{m=1}^{4}\left\{\left(H_j \cdot d\ell_j\right)_m - \left(H_{v_j} \cdot d\ell_j\right)_m\right\} + A_j \frac{3U_j^{n+1} - 4U_j^n + U_j^{n-1}}{2\Delta t}\right) \tag{14}$$

Here j locates the particular cell, m indicates cell faces and ℓ is the length of each cell face. Each variable quantity on the faces of a cell is evaluated by averaging from its values at the two control points located on the opposite sides of the cell interface.

To prevent odd-even decoupling in central-difference scheme and for stabling the numerical solution in computing high gradient of flow variables near the cavity interface, the artificial dissipation terms $D(Q_j)$ with suitable density and pressure sensors are used:

$$\frac{d}{d\tau}(Q_j A_j) + R(Q_j) - D(Q_j) = 0 \tag{15}$$

The artificial dissipation term $D(Q_j)$ is composed of two terms, respectively of second- and fourth-order differences with the coefficients which depend on the local gradients, as initially proposed by Jameson et al. [21]. The dissipation flux $D(Q_j)$ is defined as:

$$D(Q_j) = d_{i+1/2,j} - d_{i-1/2,j} + d_{i,j+1/2} - d_{i,j-1/2} \quad (16)$$

For example, $d_{i+1/2,j}$ in the above relation is a blend of first and third-order differences and it is expressed as:

$$d_{i+\frac{1}{2},j} = \frac{A_{i+1/2,j}}{\Delta\tau}\left[\varepsilon^4_{i+\frac{1}{2},j}(Q_{i+2,j} - 3Q_{i+1,j} + 3Q_{i,j} - Q_{i-1,j}) - \right. \\ \left. - \varepsilon^2_{i+\frac{1}{2},j}(Q_{i+1,j} - Q_{i,j})\right] \quad (17)$$

where ε^2 and ε^4 are the coefficients associated to second- and fourth-order artificial dissipations, respectively as

$$\varepsilon^2_{i+\frac{1}{2},j} = k_p^{(2)} \max(\delta_{i,j}, \delta_{i+1,j}) + k_\rho^{(2)} \max(\gamma_{i,j}, \gamma_{i+1,j}) \quad (18)$$

$$\varepsilon^4_{i+\frac{1}{2},j} = \max(0, k^{(4)} - \varepsilon^2_{i+\frac{1}{2},j}) \quad (19)$$

δ_{ij} and γ_{ij} are the pressure and the density sensors respectively to activate the second-difference dissipation in the regions of strong gradients such as the cavity interface, and to de-activate it elsewhere. These two sensors are defined as follows:

$$\delta_{ij} = \frac{\left|p_{i+1,j} - 2p_{i,j} + p_{i-1,j}\right|}{\left|p_{i+1,j} + 2p_{i,j} + p_{i-1,j}\right|} \quad (20)$$

$$\gamma_{ij} = \frac{\left|\rho_{i+1,j} - 2\rho_{i,j} + \rho_{i-1,j}\right|}{\left|\rho_{i+1,j} + 2\rho_{i,j} + \rho_{i-1,j}\right|} \quad (21)$$

In this study, the effects of $k_p^{(2)}$, $k_\rho^{(2)}$ and $k^{(4)}$ on the numerical results of cavitating flows are investigated.

IMPLICIT DUAL-TIME TEMPORAL DISCRETIZATION

For computing unsteady flows, explicit techniques are extremely time-consuming, since the allowable time step is much more restrictive than that needed for an acceptable level of time accuracy. Therefore, an implicit temporal discretization is required. In this study, a second-order implicit dual-time procedure is used to compute unsteady laminar cavitating flows. In this scheme, the unsteady residual should be zero at each physical time step by using an inner iterations marching at the pseudo-time [18,21]. Using the multi-stage Runge-Kutta scheme, we have:

$$Q_j^{(0)} = Q_j^{(k)}$$
$$(I + \frac{3}{2}\alpha_N \frac{\Delta\tau_j}{\Delta t} I) Q_j^{(N)} = Q_j^{(0)} - \frac{\alpha_N \Delta\tau_j}{A_j}\left(R\left(Q_j^{(N-1)}\right) - \right. \\ \left. D\left(Q_j^{(0)}\right)\right) + \frac{3}{2}\alpha_N \frac{\Delta\tau_j}{\Delta t} Q_j^{(N-1)}, \quad N = 1,2,3,4 \quad (22)$$
$$Q_j^{(k+1)} = Q_j^{(4)}$$

The parameters α_N are taken as $1/4, 1/3, 1/2$ and 1. In addition, the local time stepping is used to accelerate the convergence rate of the solution and the time step is calculated as

$$\Delta\tau = \frac{CFL \times h_i}{\lambda_{\max}} \quad (23)$$

where h_i is the minimum face size for each cell and λ_{max} is the maximum value of eigenvalues.

BOUNDARY CONDITIONS

For numerical simulation of the cavitating flows from incompressible perspective, suitable boundary conditions are required. The far field boundary conditions are used at a finite distance from the body surface. The velocity components and the density are specified at the inflow boundary and they are extrapolated at the outflow boundary, while the pressure is specified at the outflow boundary and it is extrapolated at the inflow boundary. Since the flow is viscous, no-slip condition for velocity components is enforced on the walls. The boundary conditions on the body surface are imposed by using dummy cells with appropriate values at each time step.

RESULTS AND DISCUSSION

A numerical solution of the multi-phase Navier-Stokes equation is applied to simulate steady/unsteady laminar cavitating/noncavitating flows around the two-dimensional hydrofoil. The present results are organized in two parts: The incompressible laminar flow is simulated over the NACA 0012 hydrofoil for steady and unsteady noncavitating flows and a comparison with the existing numerical results of Ref. [14] is made. The noncavitating flow condition is computed by setting a high cavitation number, i.e., $\sigma = 10.0$. Then, the results of the steady/unsteady laminar cavitating flow around the NACA 0012 hydrofoil are presented. The surface pressure distribution and convergence improvement by the preconditioning strategy are investigated. A sensitivity study is also performed to examine the effects of numerical dissipation terms on the results.

Noncavitating Flow

The numerical results of Hafez et al. [14] are used for comparison of the steady/unsteady laminar incompressible flow over the NACA 0012 hydrofoil. The geometry and the near-field details of the grid used for the computations is shown in Fig. 2. The O-grid size is (201×103) and the radius of the outlet computational domain is equal to 10 chords. In Figs. 3 and 4, the results for the surface pressure coefficient and skin friction distributions at $\mathrm{Re}_\infty = 500$ and $\alpha = 10^\circ$ are provided, respectively. For this case, the laminar flow over the hydrofoil has a steady behavior. As seen in this figures, the results are in good agreement with the other numerical results. As discussed before, a preconditioning strategy is used to ameliorate stiffness of the system of equations. Figure 5 illustrates the convergence rate of solution for the different values of the artificial compressibility parameter β for the noncavitating laminar flow over the NACA 0012 at the same conditions. It can be

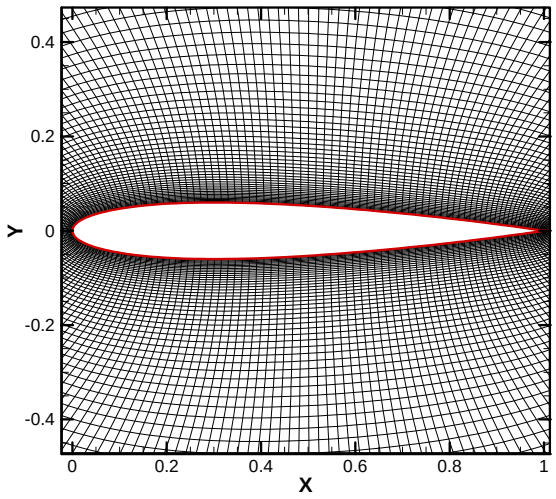

Figure 2: A close-up view of computational grid around NACA0012 hydrofoil.

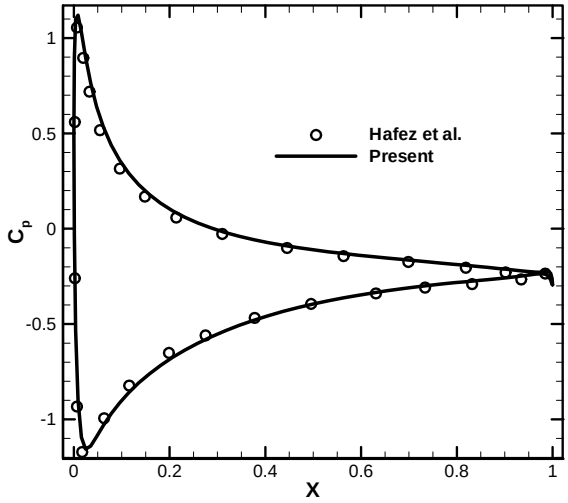

Figure 3: Comparison of the C_p distribution on the NACA 0012, noncavitating case, $\alpha = 10^{\circ}$ and $\mathrm{Re}_{\infty} = 500$.

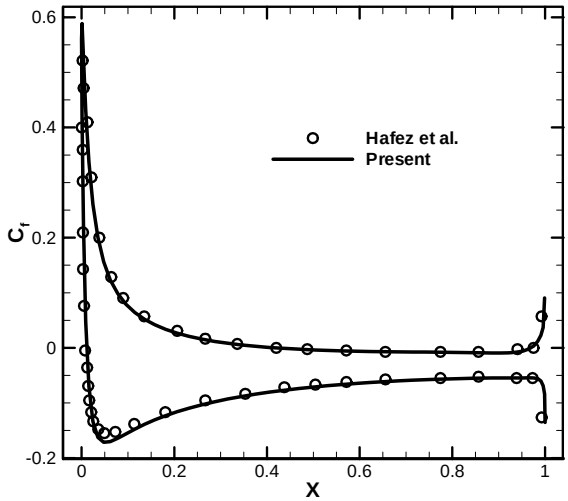

Figure 4: Comparison of the C_f distribution on the NACA 0012, noncavitating case, $\alpha = 10^{\circ}$ and $\mathrm{Re}_{\infty} = 500$.

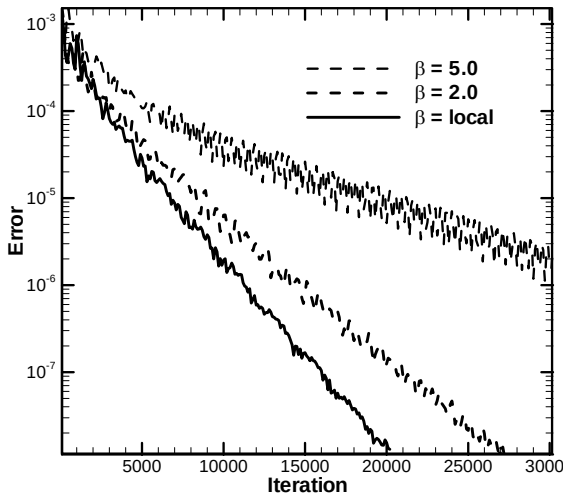

Figure 5: Convergence history of the solution for different β, noncavitating laminar flow over the NACA 0012, $\alpha = 10^{\circ}$ and $\mathrm{Re}_{\infty} = 500$.

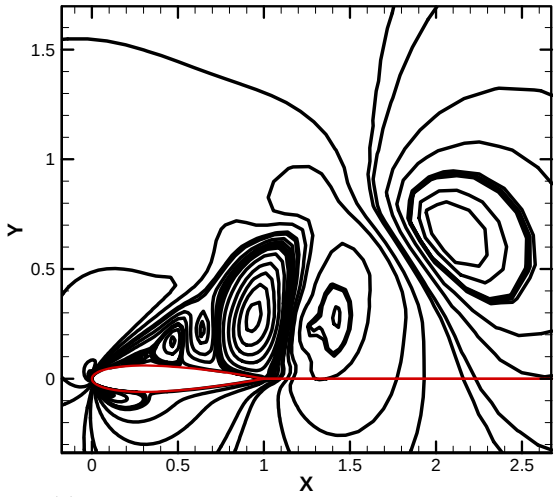

(a)

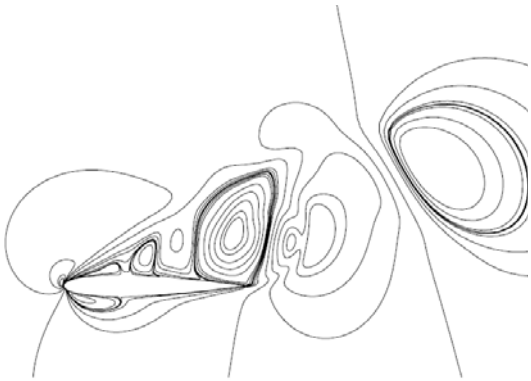

(b)

Figure 6: $v-$velocity contours on the NACA 0012, noncavitating case, $\alpha = 20^{\circ}$, $\mathrm{Re}_{\infty} = 800$ and $time = 5$. (a): Present (b): Hafez et al.

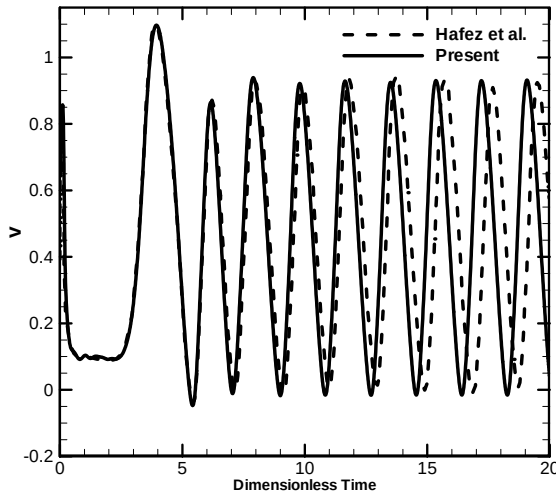

Figure 7: Comparison of time variation of the $v-$velocity at $x=1.1,\ y=0$ behind the NACA 0012, noncavitating case, $\alpha=20^{\circ}$ and $\mathrm{Re}_{\infty}=800$.

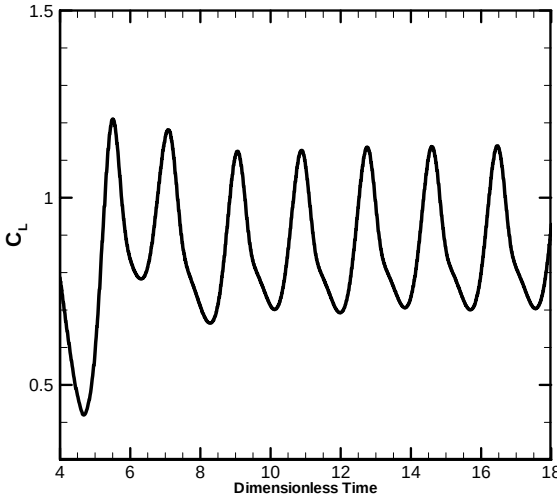

Figure 8: Lift coefficient of the NACA 0012 hydrofoil as a function of dimensionless time, noncavitating case, $\alpha=20^{\circ}$ and $\mathrm{Re}_{\infty}=800$.

seen that the convergence rate is remarkably better for local calculating β and it is shown that the preconditioning improves the convergence rate of the solution.

The results of the unsteady flow at $\mathrm{Re}_{\infty}=800$ and $\alpha=20^{\circ}$ are provided now. The present $v-$velocity contours are plotted at $t=5$ and compared with the numerical results of Ref. [14], as shown in Fig. 6. It shows the existence of a large vortex shedding towards trailing edge of the hydrofoil. The development of the $v-$velocity component with respect to the dimensionless time at point $x=1.1,\ y=0$ in the rear part of the NACA 0012 hydrofoil is given in Fig. 7. Because of the vortex shedding, the lift coefficient as shown in Fig. 8 oscillates at the Strouhal number of 0.55. Results show that the present computational method gives satisfactory agreement with the other numerical results for the simulation of steady/unsteady noncavitating laminar flows, and thus we next turn to predicate the cavitating flows for the same geometry.

Cavitating Flow

The results of the steady cavitating laminar flow over the NACA 0012 hydrofoil at $\mathrm{Re}_{\infty}=500$, $\alpha=4^{\circ}$ and the cavitation number of $\sigma=0.5$ are presented. To examine the sensitivity of the numerical solution to the dissipation parameters, the effects of the density sensor coefficient in the 2nd-order term, $k_{\rho}^{(2)}$, and the coefficient of the 4th-order dissipation term, $k^{(4)}$, on the surface pressure coefficient distribution are studied. The pressure sensor coefficient is set to be zero, $k_{p}^{(2)}=0$, because the computations have shown that this coefficient has no significant effect on the numerical simulation. Figure 9 indicates a comparison of the C_p distribution for different $k_{\rho}^{(2)}$. The coefficient of the 4th-order dissipation term is set to $k^{(4)}=1/64$ for this study. It can be seen that the coefficient of density sensor has no significant effect on the accuracy of the results of laminar cavitating flows. The small values of $k_{\rho}^{(2)}$ may lead the solution to instability, because of high gradient of the density at the cavity interface. A value of $k_{\rho}^{(2)}=1/20$ seems a suitable one for an accurate solution. With $k_{p}^{(2)}=0$ and $k_{\rho}^{(2)}=1/20$, the sensitivity of the solution to the coefficient of the 4th-order dissipation term is studied now. The effect of this coefficient on the surface pressure distribution is illustrated in Fig. 10. It is demonstrated that this coefficient has a little effect on the numerical results. The study has shown setting the value of $k^{(4)}$ to zero can cause oscillations in the solution which lead to divergence of the numerical simulation. The convergence history of the solution can be seen in Fig. 11 which shows nearly the same convergence rates for different conditions.

Fig. 12 illustrates the effect of the preconditioning coefficient α_u on the convergence rate of the solution for the cavitating laminar flow over the NACA 0012 at $\sigma=0.5$, $\alpha=4^{\circ}$ and $\mathrm{Re}_{\infty}=500$. It is concluded that the convergence rate of solution is improved with the calculation of preconditioning coefficient according to the local void fraction that it is evaluated based on the local mixture density at cavitating area. Fig. 13 shows a comparison of the pressure distribution for the present numerical solution of noncavitating and cavitating flows at different cavitation numbers over the NACA 0012 hydrofoil for $\alpha=4^{\circ}$ and $\mathrm{Re}_{\infty}=500$. The computed density contours are also shown in Fig. 14. The results indicate that the predicated cavity length increases with decreasing the cavitation number with a lower pressure after the cavity region compared to the higher cavitation number case. Note that the pressure is nearly constant (equal to the vapor pressure) in the cavity region,

With more decreasing the cavitation number or increasing the angle of attack, the cavity length and thickness are increased that cause the solution almost fluctuated and does not converge to steady state. This is because the existence a

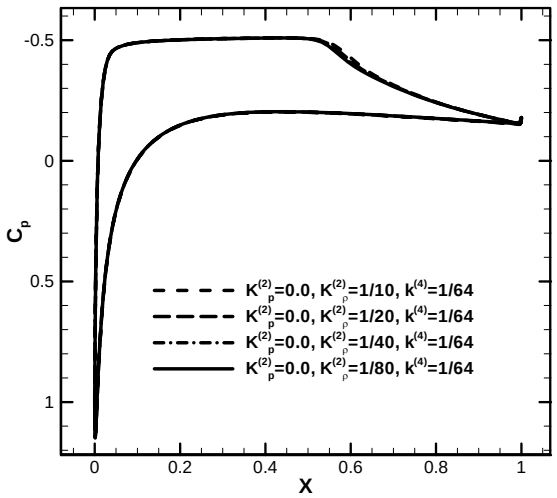

Figure 9: Comparison of the C_p distribution on the NACA 0012 hydrofoil for different 2nd-order density dissipation coefficients, cavitating case, $\sigma = 0.5$, $\alpha = 4^\circ$ and $\mathrm{Re}_\infty = 500$.

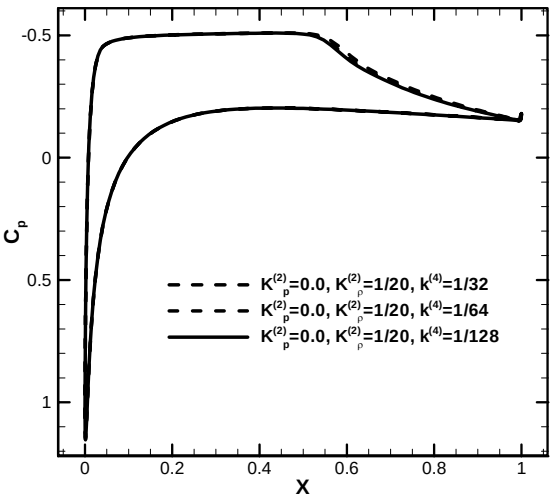

Figure 10: Comparison of the C_p distribution on the NACA 0012 hydrofoil for different 4th-order dissipation coefficients, cavitating case, $\sigma = 0.5$, $\alpha = 4^\circ$ and $\mathrm{Re}_\infty = 500$.

recirculation zone which it is injected the flow to inside the cavity from its rear lower part with the formation of a strong re-entrant jet and cause to shed bubbles. To show the overall capability and performance of the present numerical method in solving unsteady cavitating laminar flows, we perform an unsteady analysis of the cavitation over the NACA 0012 hydrofoil for different cavitation numbers and angle of attacks. The cavitation bubble collapse is a rapid phenomenon and for the study of this behavior it should employ a small time step. In this study, the dimensionless time step is set to $\Delta t = 0.0005$. In Fig. 15, one can see the density field for the several time steps at $\sigma = 0.5$, $\mathrm{Re}_\infty = 2000$ and $\alpha = 6^\circ$. The visualizations present the cloud shedding and streamlines show the development of a re-entrant jet over upper surface of the hydrofoil, which is the main reason for the periodic shedding of vapor structures downstream from a cavity. At first, the rear part of the cavity deforms and the liquid phase column moves inside the vapor phase, then the cavity is quite short and it breaks up by re-entrant jet to form a cloud cavity. The cloud cavity can arrive at the tail of the hydrofoil before collapsing. The refraction of negative pressure wave around the trailing edge of hydrofoil may cause cavitation to occur in this section of hydrofoil. In Fig. 16, the results are illustrated for $\sigma = 0.6$, $\mathrm{Re}_\infty = 2000$ and $\alpha = 10^\circ$. In this case, the cavity attached to the solid body grows up to the generation of a re-entrant jet. This leads to break-off of the downstream part of the cavity and because the angle of attack is higher than previous case, the resulting cloud of vapor is carried away by the main stream, until it enters to a higher-pressure zone and then collapses. Fig. 17 shows the variation of lift coefficient with dimensionless time for this case. The $v-$ velocity component with respect to the dimensionless time is plotted at point $x = 1.1$ and $y = 0$ in the rear part of the NACA 0012 hydrofoil in Fig. 18. The average Strouhal number of this periodical process is about 0.23. When the lift coefficient is maximum, a cavitation bubble is generated at the point of minimum pressure near the leading

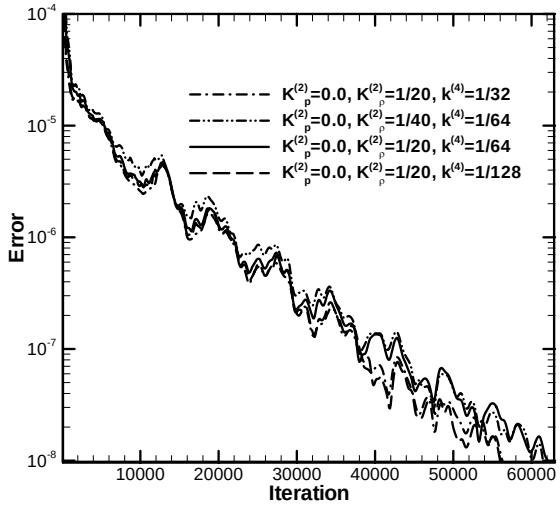

Figure 11: Convergence history of the solution for different dissipation coefficients, cavitating laminar flow over the NACA 0012, $\sigma = 0.5$, $\alpha = 4^\circ$ and $\mathrm{Re}_\infty = 500$.

edge of hydrofoil and then, it slides down the hydrofoil. When it arrives at the trailing edge of the hydrofoil, the lift decreases to a minimum and this process is repeated periodically. Some disparities in predication of cavity size and shedding frequencies were most likely due to simplifications made in the simulations, such as the assumptions of incompressible and laminar flow.

CONCLUSION

In this study, a dual-time implicit preconditioned Navier-Stokes flow solver is developed to compute the steady/unsteady laminar cavitating/noncavitating flows over hydrofoils. The cavitation physical model is based on the single-fluid approach, and the two-phase areas are considered as a single fluid, whose density is managed through a postulated barotropic state law.

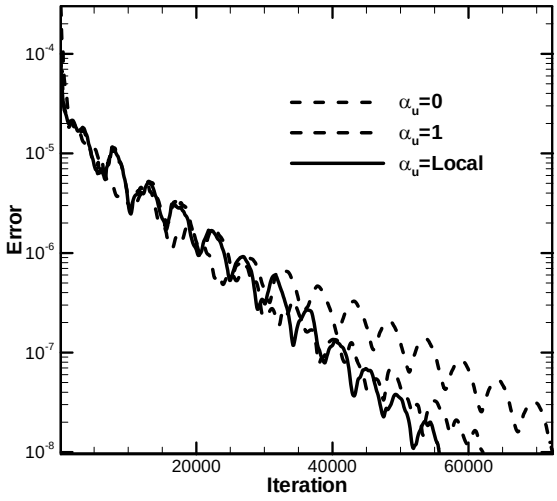

Figure 12: Convergence history of the solution for different α_u, cavitating laminar flow over the NACA 0012 hydrofoil, $\sigma = 0.5$, $\alpha = 4^\circ$ and $\mathrm{Re}_\infty = 500$.

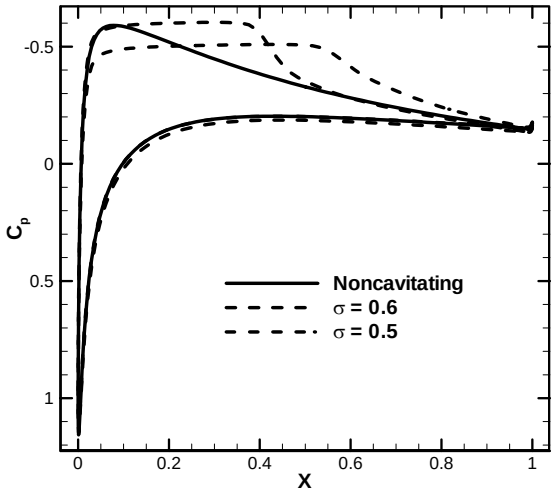

Figure 13: Comparison of the C_p distribution for the NACA 0012 hydrofoil at different cavitation numbers, $\alpha = 4^\circ$ and $\mathrm{Re}_\infty = 500$.

To ameliorate the difficulty due to the stiffness of the system of equations and improve the performance of the numerical treatment in modeling cavitating flows, a preconditioning strategy is used. A cell-centered finite-volume scheme employing the suitable dissipation terms to account for density jumps across the cavity interface is shown to yield an effective method for solving the multiphase Navier-Stokes equations. A second-order implicit dual-time procedure is used to compute unsteady laminar cavitating/noncavitating flows. The accuracy of the results is verified by comparison with the available numerical results. Although, the preconditioning procedure presented may be used for different cavitation models, the performance of the numerical treatment should be checked through numerical experiments. The study demonstrates that the multiphase Navier-Stokes flow solver developed can be used for the simulation of steady/unsteady laminar cavitating/noncavitating flows over 2D hydrofoils.

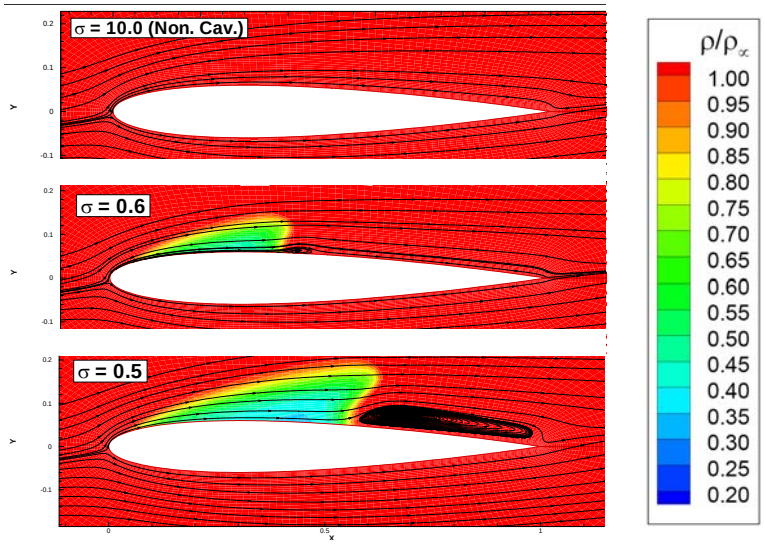

Figure 14: Density contours over the NACA 0012 hydrofoil at different cavitation numbers, $\alpha = 4^\circ$ and $\mathrm{Re}_\infty = 500$.

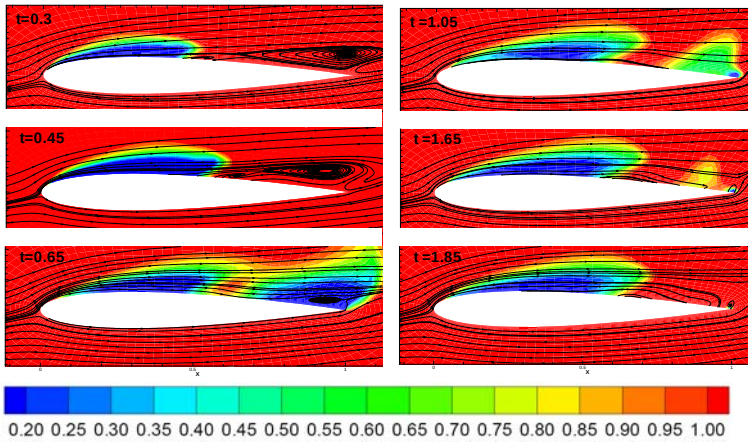

Figure 15: Evolution of the density field around NACA0012 hydrofoil at $\sigma = 0.5$, $\mathrm{Re}_\infty = 2000$ and $\alpha = 6^\circ$.

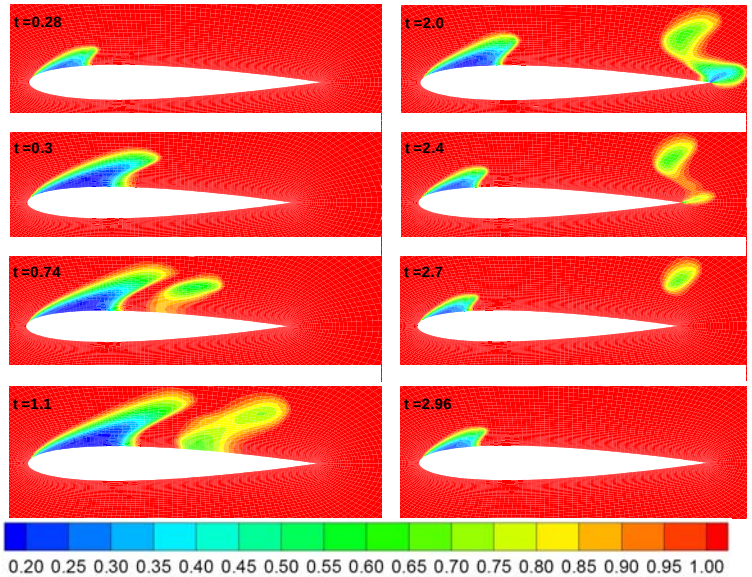

Figure 16: Evolution of the density field around NACA0012 hydrofoil at $\sigma = 0.6$, $\mathrm{Re}_\infty = 2000$ and $\alpha = 10^\circ$.

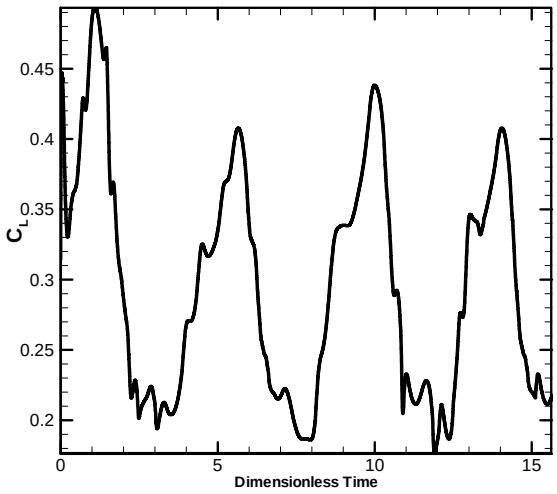

Figure 17: Lift coefficient of the NACA 0012 hydrofoil as a function of dimensionless time, unsteady cavitating case, $\sigma = 0.6$, $\mathrm{Re}_\infty = 2000$ and $\alpha = 10^\circ$.

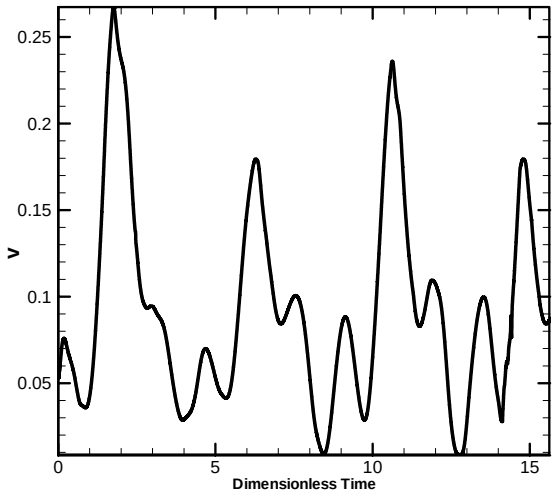

Figure 18: The v – velocity component at $x = 1.1$, $y = 0$ behind the NACA 0012 hydrofoil, unsteady cavitating case, $\sigma = 0.6$, $\mathrm{Re}_\infty = 2000$ and $\alpha = 10^\circ$.

REFERENCES

[1] Kueny, JL., Schultz, F., and Desclaud, J. 1988, "Numerical prediction of partial cavitation in pumps and inducers," *IAHR Symposium*, Trondheim.

[2] Kubota, A., Kato, H., and Yamaguchi, H. 1992, "A new modelling of cavitating flows: a numerical study of unsteady cavitation on a hydrofoil section," *Journal of Fluid Mechanics*; 240, 59–96.

[3] Delannoy, Y., and Kueny, JL. 1990, "Two phase flow approach in unsteady cavitation modeling," *Cavitation and Multiphase Flow Forum, ASME-FED*, 98, 153–158.

[4] Merkle, CL., Feng, J., and Buelow, PEO. 1998, "Computational modelling of the dynamics of sheet cavitation," *3rd International Symposium on Cavitation*, Grenoble, France.

[5] Song, C., and He, J. 1998, "Numerical simulation of cavitating flows by single-phase flow approach," *3rd International Symposium on Cavitation*, Grenoble, France.

[6] Arndt, R.E.A., Song, C.C.S., Kjeldsen, M., He, J. and Keller, A., "Instability of Partial cavitation: A Numerical/Experimental Approach," *23 rd Symposium on Naval Hydrodynamics*, Rouen, France.

[7] Reboud, JL., Stutz, B., and Coutier, O. 1998, "Two phase flow structure of cavitation: experiment and modelling of unsteady effects," *3rd International Symposium on Cavitation*, Grenoble, France.

[8] Coutier-Delgosha, O., Reboud, JL., and Albano, G. 2000, "Numerical simulation of the unsteady Cavitation behaviour of an inducer blade cascade," *ASME FEDSM00*, Proceedings.

[9] Coutier-Delgosha, O., Fortes-Patella, R., and Reboud, JL. 2002, "Evaluation of the turbulence model influence on the numerical simulations of unsteady cavitation," *Journal of Fluid Engineering*; 125, 38–45.

[10] Kunz, R., Boger, D., Chyczewski, T., Stinebring, D., and Gibeling, H. 1999, "Multi-phase CFD analysis of natural and ventilated cavitation about submerged bodies," *3rd ASME=JSME Joint Fluids Engineering Conference*, San Francisco.

[11] Frobenius, M., Schilling, R., Friedrichs, J., and Kosyana, G. 2002, "Numerical and experimental investigation of cavitating flow in a centrifugal pump impeller," *ASME Fluid Engineering Division Summer Meeting*.

[12] Ventikos, Y., and Tzabiras, G. 2000, "A numerical method for the simulation of steady and unsteady cavitating flows," *Journal of Computer & Fluids*, pp. 63-88.

[13] Coutier-Delgosha, O., Fortes-Patella, R., Reboud, J.L., Hakimi, N., and Hirsch, C. 2005, "Stability of preconditioned Navier-Stokes equations associated with a cavitation model," *Journal of Computers and Fluids*, 34, 319-349.

[14] Hafez, M., Shatalov, A., and Nakajima, M. 2007, "Improve numerical simulations of incompressible flows based on viscous/inviscid interaction procedures," *Journal of Computers and Fluids*, pp. 1588-1591.

[15] Chorin, A. J., 1967, "A Numerical Method for Solving Incompressible Viscous Flow Problems," *J. of Computational Physics*, pp. 12-26.

[16] Ahuja, V., Hosangadi, A., and Aruanajatesan, S. 2001, "Simulations of Cavitating Flows Using Hybrid Unstructured Meshes," *to be Published in Journal of Fluids Engineering*.

[17] Turkel, E. 1993, "Review of preconditioning methods for fluid dynamics," *J Appl Numer Math.*

[18] Jameson, A., 1991, "Time Dependent Calculations Using Multigrid, with Application to Unsteady Flows Past Airfoils and Wings," *AIAA paper 91-1596.*

[19] Jameson, A., 1991, "Time Dependent Calculations Using Multigrid, with Application to Unsteady Flows Past Airfoils and Wings," *AIAA paper 91-1596.*

[20] Pascarella, C., and Salvatore, V., 2003, “Effect of Speed of Sound Variation on Unsteady Cavitation Flows by Using a Barotropic Model,” *Fifth International Symposium on Cavitation (cav2003)*, Osaka, Japan.

[21] Jameson, A., Schmidt, W., and Turkel, E. 1981, “Numerical solutions of the Euler equations by finite volume methods using Runge-Kutta time-stepping schemes,” *AIAA Paper*, 81–1259.